International Journal for Housing Science and Its Applications
Publish August 5, 2025. Volume 46, Issue 3 Pages 3945-3957

https://doi.org/10.70517/ijhsa463335

Design of grid wide area protection scheme based on optimization algorithm and real-time monitoring system

Yu Sui[1], Xun Lu[2], Xiaoyu Deng[1] and Wei Xu[1,*]

[1] Power Grid Planning Research Center of Guangdong Power Grid Co., Ltd., Guangzhou, Guangdong, 510220, China
[2] Guangdong Power Grid Co., Ltd., Guangzhou, Guangdong, 510600, China

Corresponding authors: (e-mail: SuiYu202412@126.com).

Abstract The expansion of power grid scale puts forward higher requirements on the maintenance and protection level of power grid. This paper focuses on the idea of "architecture design - data processing - optimization solution" to carry out research. Layered system architecture is designed, and multi-module combination realizes the transmission of data flow, real-time data pre-processing and dimensional analysis, and solves the problem of the difference of the magnitude and the phase angle jumping. The Fourier algorithm is chosen to discretize the AC sampling data, and the discrete Fourier transform algorithm reduces the computational redundancy and ensures the computational accuracy and speed. The improved TLBO algorithm is proposed to realize the global coordinated optimization of WAPSS parameters through the elite reservation strategy and dynamic parameter update mechanism. Comparison experiments are utilized to verify the effectiveness of the proposed method. The results show that the three error indicators of steady state recording error, current measurement accuracy, and three-phase phase difference value of the algorithm in this paper do not exceed the specified ranges of 0.55A, 0.55%, and 0.55. The network loss of the system after algorithm optimization decreases to 1.841MW, and the calculation time is only 12.1s, which is better than the comparison algorithm. The parameter optimized motor angle of attack difference is smaller and the fluctuation is smoother.

Index Terms grid wide-area protection, data dimensionality reduction, real-time stream processing, full perimeter wave Fuchs algorithm, improved TLBO algorithm

I. Introduction

Since the 21st century, with the construction of strong smart grid and the rapid development of network communication technology, optoelectronic technology and other related technologies, the operation mode of the substation is gradually changing, and the intelligent substation has emerged [1]-[3]. Especially in China in recent years, intelligent substation technology has been developed rapidly, and many intelligent substation pilots have been established across the country. The operation mode of large power grids puts forward higher requirements for the protection and control of power systems [4]. Since the action criteria used in traditional relay protection are usually based on local measurement information, they can only reflect the limited operation status at a certain point or a small area in the power system, and are unable to grasp the network-wide operation status information, thus failing to ensure the safe and stable operation of the whole bureau [5]-[8]. Therefore, it is appropriate to adopt protection control based on wide-area information in the field of intelligent substation.

With the development of computer, network, communication, intelligent equipment and other technologies and the progress of power grid control theory, the secondary specialties involved tend to integrate with each other, and it has become an inevitable trend to configure various applications from the overall consideration of the secondary system [9]-[11]. Combined with the technological development of the station secondary system configuration program research, the current monitoring, control, safety and stability, protection and other functions to optimize the combination, in order to form a highly integrated secondary system [12], [13]. In the highly integrated secondary integration system, based on the integration of protection functions, wide-area information is introduced into the protection system to solve the problems that are difficult to be solved by conventional protection using local information [14]-[16]. Based on the above concepts, it is necessary to study and develop the network protection system device based on the concept of wide-area integration, and put the system into the actual test [17], [18].

In order to improve the data processing efficiency and solution accuracy in the design of grid wide-area protection scheme, this paper constructs a wide-area measurement and analysis system based on data dimensionality reduction. The combination of sliding window sampling and full perimeter wave Fuchs algorithm realizes high quality and efficient processing of sampled data. The parameters of the wide-area power system stabilizer WAPSS are co-

optimized in two stages using the improved TLBO algorithm to improve the grid protection effect. The effect of the sampling data processing algorithm is measured by error detection tests in terms of steady state recording error, current measurement accuracy, and three-phase phase difference value. Conduct comparison experiments to verify the advantages of the grid protection scheme of the optimization algorithm. Compare the size and fluctuation range of the motor power angle difference before and after parameter optimization to determine the importance of parameter optimization.

II. Technical support related to the design of a wide-area protection program for the power grid

This chapter details how to obtain the optimal results of the grid wide protection scheme from the dimensions of system architecture, data processing, and optimization solution.

II. A. Wide-area measurement analysis

II. A. 1) System architecture

In this paper, we propose an analysis system for massive real-time wide-area measurement data, which utilizes data dimensionality reduction to perform steady-state assessment of power grids with high processing efficiency and real-time performance. Figure 1 shows the specific system framework. In the data computation and analysis platform, the system mainly performs the following operations: data preprocessing, sliding window sampling and dimensionality reduction analysis. The input data stream first enters the preprocessing process, after which the system performs sliding window sampling on the output data stream. The sampled data can form a two-dimensional matrix and input to the dimensionality reduction algorithm for dimensionality reduction analysis. The component modules of each process are as follows:

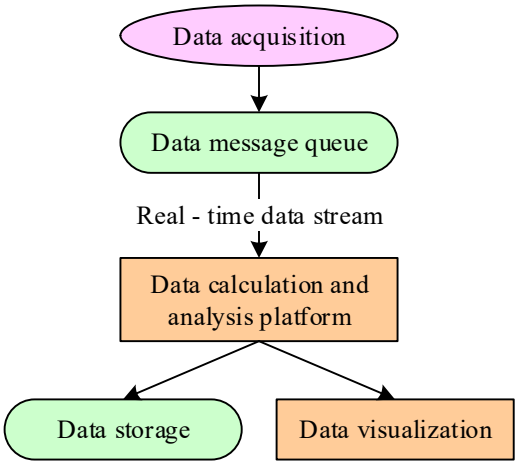

Figure 1: System Architecture

1) Data acquisition module for acquiring massive real-time wide-area measurement data from said data source using Web or ETL.

2) Data message queue for employing frameworks such as Apache Kafka,ZeroMQ, etc., to persist the said data until they have been fully processed to avoid the risk of data loss.

3) Data computation and analysis platform, which is used for real-time stream processing frameworks such as Apache Storm, Apache Spark Streaming, Apache Samza, etc., to carry out data preprocessing, sliding-window sampling, and dimensionality reduction operations on real-time streaming data of voltage phase angle collected by the wide-area measurement system, and to judge the steady state condition of the grid based on the results of the dimensionality reduction. The methods include but are not limited to singular value decomposition.

4) Data visualization module, which is used to draw graphical display and security warning of various data including the above analysis and calculation results by using Web page, PC client and cell phone APP display form.

5) Data storage module, used to use HDFS and other ways, including the above analysis of the results of the operation of various data data access operations.

II. A. 2) Data pre-processing

In the real-time streaming data collected by the wide-area measurement system, the voltage and phase angle have different magnitudes and value ranges, and the direct dimensionality reduction operation on them will lead to uneven spatial distribution, which in turn affects the analysis results. In addition, in the polar coordinate space composed of u and θ, a voltage vector rotating around the origin will cause the value of θ to jump from 0°~360° or 360°~0° when it passes through the $(1,0)$ vector, which will also affect the results. Therefore, a preprocessing operation is required.

The conventional method is to normalize or regularize the data. Normalization begins by assuming that each feature in the sample obeys a normal distribution, and then transforms the features into the form of a standard normal distribution according to $x=(x-\mu)/\sigma$. Regularization then scales the value of each sample so that its unit paradigm is 1. It can be seen that neither of these methods is applicable to the preprocessing of PMU data with time series as input parameters. Therefore, let the voltage be u and the phase angle be θ, using Eq:

$$\begin{cases} u^r = u\cdot\cos\theta \\ u^i = u\cdot\sin\theta \end{cases} \tag{1}$$

It is converted into the form of real voltage V^r and imaginary voltage V^i, which have the same range of values of voltage and phase angle and have the same magnitude, which achieves the effect of data normalization while retaining all the information. Then, let u_0^r and u_0^i of the initial moment be the basis vectors, and for each moment, let

$$\begin{cases} u_t^r = u_t^r - u_0^r \\ u_r^i = u_t^i - u_0^i \end{cases} \tag{2}$$

This eliminates the bias of each input time series so that they have the same distribution. Physically, this is equivalent to eliminating the effect of the initial state on the results.

II. B.Sampling data processing algorithm

The types of analog quantities in grid systems and power plants and substations are AC, DC, and non-electric quantities. In this paper, we choose the AC sampling method to sample the analog quantity. AC sampling is to directly sample the waveforms of AC current and voltage, and then calculate their RMS values and phases through certain algorithms, and calculate quantities such as active power and reactive power. Main features:

1) Good real-time. It can avoid the influence of the large time constant of the rectifier and filter link in DC sampling, which is suitable for the case of high sampling requirements.

2) It can reflect the actual waveform of the original current and voltage, which is convenient for waveform analysis of the measured results, and is suitable for occasions requiring harmonic analysis or fault recording.

3) The active power and reactive power are calculated by sampling the current and voltage, so the active power and reactive power transmitter can be eliminated, saving investment and reducing the size of the equipment.

4) The conversion rate of the A/D converter and the sampling keeper have high requirements. In order to ensure the accuracy of the measurement, in the same cycle, must ensure that there are enough sampling points, so the A/D converter is required to have sufficient conversion speed.

5) Measurement accuracy depends not only on the hardware performance of the analog input channel, but also on the software algorithm, so the sampling and calculation procedures are more complex.

The core problem of the software algorithm related to AC sampling is to convert the continuous current and voltage input signals into digital quantities that can be processed by computers through discrete sampling and analog-to-digital conversion, and then calculate the physical quantities that can characterize the operating characteristics of the monitored object. The criteria for analyzing and evaluating the advantages and disadvantages of different algorithms are accuracy and speed. Accuracy is the error between the calculated value and the actual value; speed is the length of the data window required in the calculation speed includes two aspects: first, the length of the data window required by the algorithm (or the number of sampling points); and second, the algorithm operation workload.

The system uses the full perimeter Fuchs algorithm for synchronized phase measurement. The full-wave Fourier algorithm (DFT method) through the measured voltage, current discrete sampling points for Fourier transform, to find the voltage, current phase quantity of the effective value and its phase angle.

Let the input signal be:

$$X(t)=A\sin\left(2\pi ft+\theta\right) \tag{3}$$

Express it in the form of a complex exponential:

$$X(t)=\frac{A}{2j}\left(e^{j2\pi ft}e^{j\theta}-e^{-j2\pi ft}e^{-j\theta}\right) \tag{4}$$

Its sampling value is:

$$\begin{aligned} x\left(kT_s\right) &= A\sin\left(2\pi fkT_s+\theta\right) \\ &= A\sin\left(2\pi k/N+\theta\right) \quad k=0,1,2,\cdots(N-1) \end{aligned} \tag{5}$$

Its complex exponential form is:

$$x(k)=A\frac{e^{j\left(\frac{2\pi}{N}k+\theta\right)}-e^{-j\left(\frac{2\pi}{N}k+\theta\right)}}{2j} \tag{6}$$

A discrete Fourier transform of Eq. (6) yields:

$$\begin{aligned} \vec{X} &= \frac{2j}{N\sqrt{2}}\sum_{k=0}^{N-1}x(k)e^{-j\frac{2\pi}{N}k} \\ &= \frac{A}{N\sqrt{2}}\sum_{k=0}^{N-1}\left(e^{jC}-e^{-jD}\right) \end{aligned} \tag{7}$$

Among them:

$$C=\theta,\quad D=\frac{4\pi}{N}k+\theta \tag{8}$$

So there is a phase X:

$$\bar{X}=\frac{A}{\sqrt{2}}e^{j\theta}-\frac{A}{N\sqrt{2}}e^{-j\theta}\sum_{k=0}^{N-1}\left(e^{-j\frac{4\pi}{N}k}\right) \tag{9}$$

Consider:

$$\sum_{k=0}^{N-1}\left(e^{-j\frac{4\pi}{N}k}\right)=0 \tag{10}$$

And so it gets:

$$\vec{X}=\frac{A}{\sqrt{2}}e^{j\theta} \tag{11}$$

The microcomputer implementation of the above algorithm is to write equation (11) in the following form:

$$\begin{aligned} \vec{X} &= \frac{2j}{N\sqrt{2}}\sum_{k=0}^{N-1}x(k)e^{-j\frac{2\pi}{N}k} \\ &= \frac{2j}{N\sqrt{2}}\sum_{k=0}^{N-1}\left[x(k)\cos\left(\frac{2\pi}{N}k\right)-jx(k)\sin\left(\frac{2\pi}{N}k\right)\right] \\ &= \frac{1}{\sqrt{2}}\left(X_{s0}+jX_{c0}\right) \end{aligned} \tag{12}$$

Among them:

$$\begin{aligned} X_{s0} &= \frac{2}{N}\sum_{k=0}^{N-1}\left[x(k)\sin\left(\frac{2\pi}{N}k\right)\right]=A\cos\theta \\ X_{c0} &= \frac{2}{N}\sum_{k=0}^{N-1}\left[x(k)\cos\left(\frac{2\pi}{N}k\right)\right]=A\sin\theta \end{aligned} \tag{13}$$

Figure 2 shows how the DSP system is realized. L_1, L_2 is the sequence of sampling points (set one week wave 63 points sampling), S_1 is the corresponding angle sine value stored in FLASH, which is connected to form a closed loop. When calculating X_{S0}, the sequence of sampling points moves to the right in the direction shown by the arrow, and S_1 moves upward in the direction shown by the arrow X_{S0}, which constitutes a closed loop through the arrow on the left. Since the cosine and sine values of the angle are symmetric about $\pi/2$, the computation of X_{C0} starts from the seventeenth frame of S_1, and S_1 moves downward in the direction shown by the arrow X_{C0}, forming a closed loop through the arrow on the right. The sequence of sampling points L_2 still moves to the right in the direction shown by the arrow.

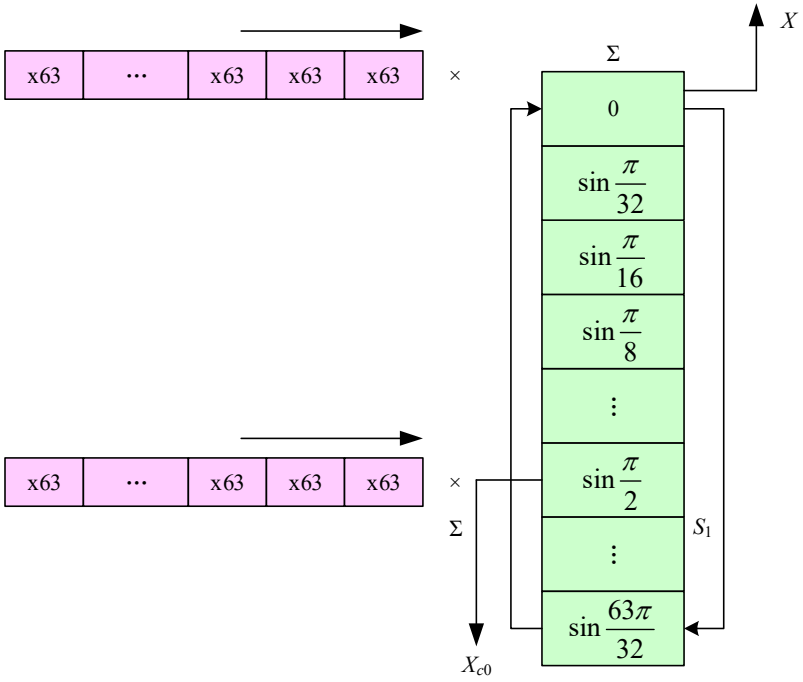

Figure 2: Implementation method of DSP system

The above is the result of calculating the sampling points $k=0,1,\cdots,N-1$ for the first data window, and it is not difficult to show that the phase X obtained from the calculation for the r th data window will be turned counterclockwise in the complex plane by an angle of $r*(2\pi/N)$. Since each new data window differs from the old data window by only two points of data, the first point of the previous data window and this point of the latest sampling of the current data window, the measurement device can use a recursive algorithm.

When calculating the r th data window, it is given by equation (13):

$$\begin{aligned} X_{s(r)}^{(\theta)} &= \frac{2}{N}\sum_{k=0}^{N-1} x_{k+r}\sin\left(\frac{2\pi}{N}k+\frac{2\pi}{N}r\right) \\ &= \frac{2}{N}\sum_{k=0}^{N-1} x_{k+r}\sin\left[\frac{2\pi}{N}(k+r)\right] \end{aligned} \tag{14}$$

Order $k'=k+r$

$$\begin{aligned} X_{s(r)}^{(\theta)} = \frac{2}{N}\Bigg[\sum_{k'=r-1}^{N+r-2} x_{k'}\sin\left(\frac{2\pi}{N}k'\right)+x_{N+r-1} \\ \sin\frac{2\pi}{N}(N+r-1)-x_{r-1}\sin\frac{2\pi}{N}(r-1)\Bigg] \end{aligned} \tag{15}$$

Order $k=k'-(r-1)$

$$X_{s(r)}^{(\theta)}=\frac{2}{N}\left[\sum_{k=0}^{N-1}x_{k+(r-1)}\sin\frac{2\pi}{N}(k+r-1)\right.$$
$$\left.+x_{N+r-1}\sin\frac{2\pi}{N}(N+r-1)-x_{r-1}\sin\frac{2\pi}{N}(r-1)\right] \tag{16}$$

Calculated from the $r-1$ th data window $X_{s(r-1)}^{(\theta)}=\frac{2}{N}\sum_{k=0}^{N-1}\left[x_{k+(r-1)}\sin\frac{2\pi}{N}(k+r-1)\right]$ Then

$$X_{s(r)}^{(\theta)}=X_{s(r-1)}^{(\theta)}+\frac{2}{N}(x_{N+r-1}-x_{r-1})\sin\frac{2\pi}{N}(r-1) \tag{17}$$

Ditto:

$$X_{c(r)}^{(\theta)}=X_{c(r-1)}^{(\theta)}+\frac{2}{N}(x_{N+r-1}-x_{r-1})\cos\frac{2\pi}{N}(r-1) \tag{18}$$

$$\therefore\ \overrightarrow{X_r}=\overrightarrow{X_{r-1}}+j\frac{\sqrt{2}}{N}(x_{N+r-1}-x_{r-1})e^{-j\frac{2\pi}{N}(r-1)} \tag{19}$$

Therefore, when calculating the phase of the r th data window, it is not necessary to calculate the cumulative sum of the 63 sampling points, but just calculate the new point added to the r th data window and the first sampling point dropped in the $r-1$ th data window according to equation (19). At the same time, from equation (19), it can also be seen that if the frequency of the sampled wave remains constant, i.e., 63 points are sampled at equal intervals to sample exactly the complete wave, then the sampling point $x_{N+r-1}=x_{r-1}$, so the phase volume calculated in the r th data window coincides exactly with that obtained in the $(r-1)$ th data window, and therefore the result of the recursive discrete Fourier transform algorithm is a compound phase quantity stationary in the plane.

The starting data window of the discrete Fourier transform algorithm is the sampling points of a weekly wave, so its calculation period is a weekly wave, and from the second data window, every sampling point can be calculated once, so the recursive discrete Fourier transform algorithm has a shorter time period. The discrete Fourier transform algorithm has a very good filtering characteristics, the method of calculating the fundamental phase using the DFT algorithm discussed above can be easily extended to the calculation of the 0th ~ 30th harmonics (assuming a weekly wave of 63 points sampling). The discrete Fourier transform algorithm can directly obtain the voltage and current phasors (including RMS and phase angle), and the power calculation becomes very convenient due to the obtaining of the voltage and current phasors.

Calculation of other values:

The phase angle of the signal fundamental: $\delta=\arctan(X_{c0}/X_{s0})$.

The inverse function is accomplished using the look-up table method in the DSP system implementation.

The amplitude of the signal fundamental: $A=X_{s0}/\cos\delta$.

In the DSP system implementation use the look-up table method to complete the operation of $1/\cos\delta$.

Base wave active/reactive power subranges

A Phase fundamental waveforms

$$S_A=U_AI_A=(U_{s0A}+jU_{c0A})(I_{s0A}-jI_{c0A})$$
$$=(U_{s0A}\times I_{c0A}+U_{s0A}\times I_{c0A})$$
$$+j(U_{s0A}\times I_{c0A}-U_{s0A}\times I_{c0A}) \tag{20}$$

Single-phase active power:

$$P_A=U_{c0A}\times I_{s0A}+U_{c0A}\times I_{s0A} \tag{21}$$

Single-phase reactive power:

$$Q_A=U_{c0A}\times I_{s0A}-U_{c0A}\times I_{s0A} \tag{22}$$

Three-phase active power:

$$P=P_A+P_B+P_C \tag{23}$$

Three-phase reactive power:

$$Q = Q_A + Q_B + Q_C \tag{24}$$

Base wave power factor angle:

$$\phi = \arctan\left(Q / P\right) \tag{25}$$

Zero sequence current:

$$I_{0s0} = I_{s0A} + I_{s0B} + I_{s0C} \tag{26}$$

$$I_{0c0} = I_{c0A} + I_{c0B} + I_{c0C} \tag{27}$$

$$I_0 = \sqrt{I_{0c0}^2 + I_{0s0}^2} \tag{28}$$

Straight traffic:

$$U_d = \frac{1}{N}\sum_{k=0}^{N-1} u(k) \quad I_d = \frac{1}{N}\sum_{k=0}^{N-1} i(k) \tag{29}$$

where $u(k)$ and $i(k)$ are the sampling values of voltage and current.

II. C. Two-stage coordinated optimization of WAPSS parameters based on improved TLBO algorithm

In this paper, we propose a two-stage coordinated optimization method for WAPSS parameters based on the TLBO algorithm, which uses the improved TLBO algorithm to optimize the gain of WAPSS in the following steps:

1) Create an initialized population according to Equation (30) with $X_e = [K_1, K_2, \cdots, K_{ei}, \cdots, K_d]$. X_e is the eth vector in the population $(e \in [1, D])$, which represents a vector consisting of a set of variables to be optimized, and D is the dimension of X. K_{ei} is the eith element of X_e, representing the gain of the PSS, and d is the number of PSSs $(ei \in [1, d])$. In addition, in order to make the optimization problem have an initial feasible solution while reducing the number of iterations, the individuals in the initial population X_e include individuals consisting of the critical amplification gains of the units in addition to those generated by the random function:

$$K_{ei} = K_{\min} + rand \times \left(K_{\max} - K_{\min}\right) \tag{30}$$

In Eq. (30), $rand$ is a random number ranging from 0 to 1, the same below.

2) Substitute X_e into the objective function to calculate the fitness $F(X_e)$ of the initial population. The $F(X_e)$ measures the merit of the initial solution, and the best individual X_{best} and N_{es} elite solutions are selected from X_e and retained according to the size of $F(X_e)$;

3) Calculate the mean value X_{mean} of all gains in the population and its difference from X_{best} as shown in equation (31);

$$difference = rand \times \left(X_{best} - round\left[1 + rand(0,1)\right] \times X_{mean}\right) \tag{31}$$

4) For each body X_e, update the gain of the PSS according to X_{best} and $difference$ as shown in Equation (32);

$$\begin{cases} X_e^{new} = X_e^{old} + difference \\ if\ F\left(X_e^{new}\right) F\left(X_e^{old}\right) \\ X_e^{new} = X_e^{old} \end{cases} \tag{32}$$

In Eq. (32), X_e^{new} and X_e^{old} are the values of X_e before and after updating, respectively.

5) Two individuals X_{e1} and X_{e2} are randomly selected to compare the difference in fitness between X_{e1} and X_{e2} and update the PSS gain as shown in Equation (33);

$$X_{e1}^{new} = \begin{cases} X_{e1} + rand \times (X_{e1} - X_{e2}), & F(X_{e1}) < F(X_{e2}) \\ X_{e1} + rand \times (X_{e2} - X_{e1}), & F(X_{e2}) < F(X_{e1}) \end{cases} \tag{33}$$

6) Replace the N_{es} worst individual using an elite solution to increase the fitness level of the population;
7) End the optimization process after reaching the maximum number of iterations or convergence objective.

III. Analysis of the application and effectiveness of wide-area protection technologies for power grids

In this chapter, the proposed sampling data processing algorithm, optimization method and parameter optimization effect are verified to judge the application value of this paper's method in power grid wide area protection.

III. A. Examination of the error situation of the sampling data processing algorithm

III. A. 1) Steady-state recording error test

Using the algorithm in this paper, the data obtained from sampling is processed to obtain data that can be analyzed and calculated by a computer. In order to prove the effectiveness of the algorithm, the various types of processed values are analyzed for their usability through an error case test. Table 1 shows the results of the steady state recording error test. Steady-state recording error test requirements: measurement range of 0A ~ 650A; error: 0 ⩽ I < 150, no more than 0.55A; 150 ⩽ I < 630, no more than 0.55%. From the test results, when 0 ⩽ I < 150, the error of the three channels is maximum 0.20A, less than 0.55A; when 150 ⩽ I < 630, the error is maximum 0.20%, also less than 0.55%. Therefore, the test results are qualified, and the steady state recording error of the data processed by the algorithm of this paper is within the acceptable range.

Table 1: Steady-state recording error test results

Channel	Applied value (A)	Display value (A)	Error
A	0	0.0	0.00A
	50	49.9	0.10A
	150	150.1	0.07%
	250	250.1	0.04%
	350	350.3	0.09%
	450	450.4	0.09%
	550	550.2	0.04%
	650	650.3	0.05%
B	0	0.0	0.00A
	50	50.2	0.20A
	150	150.3	0.20%
	250	250.4	0.16%
	350	350.5	0.14%
	450	450.4	0.09%
	550	550.1	0.02%
	650	650.2	0.03%
C	0	0.0	0.00A
	50	50.1	0.10A
	150	150.2	0.13%
	250	250.3	0.12%
	350	350.4	0.11%
	450	450.4	0.09%
	550	550.1	0.02%
	650	650.1	0.02%

III. A. 2) Current measurement accuracy test

Current measurement accuracy test requirements: measurement range of 0A ~ 650A; 0 ⩽ I < 150, the measurement error does not exceed 0.55A; 150 ⩽ I < 650, the measurement error does not exceed 0.55%. Table 2 shows the current measurement accuracy test results. According to the test results, when 0⩽I<150, the maximum error is 0.30A; when 150⩽I<650, the maximum error is 0.24%, all of which exceed the maximum error range. The test results are qualified. The adopted data processed by the algorithm in this paper meets the current measurement accuracy requirements.

Table 2: Test results of current measurement accuracy

Channel	Applied value (A)	Display value (A)	Error
A	0	0.0	0.00A
	50	49.8	0.20A
	150	150.2	0.13%
	250	250.2	0.08%
	350	350.4	0.11%
	450	450.5	0.11%
	550	550.1	0.02%
	650	650.2	0.03%
B	0	0.0	0.00A
	50	50.1	0.10A
	150	150.2	0.13%
	250	250.3	0.12%
	350	350.5	0.14%
	450	450.2	0.04%
	550	551.3	0.24%
	650	650.3	0.05%
C	0	0.0	0.00A
	50	50.3	0.30A
	150	150.2	0.13%
	250	250.1	0.04%
	350	350.2	0.06%
	450	450.3	0.07%
	550	551.2	0.22%
	650	650.4	0.06%

III. A. 3) Three-phase phase difference test

Three-phase phase difference value test requirements: three-phase phase difference value absolute value $\leqslant$ 0.55. Figure 3 is the three-phase phase difference value results. From the difference curve in the figure, it can be seen that the absolute value of A-B and A-C phase difference value is 0.2, and the absolute value of B-C phase difference value is 0.3. The absolute value of the three-phase phase difference value does not exceed 0.55, and the test result is qualified. This paper's algorithm processing after the adoption of data to meet the three-phase phase error requirements.

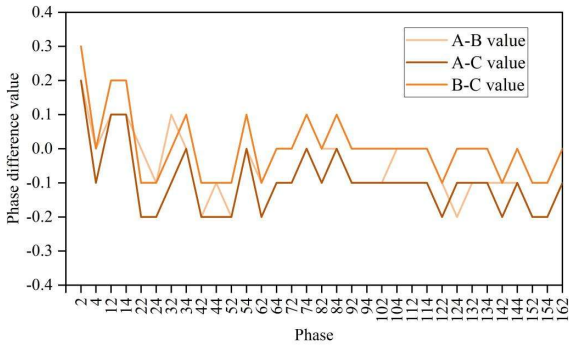

Figure 3: The result of three-phase phase difference

III. B. Validation of the effectiveness of the optimization method

III. B. 1) Analysis of the effectiveness of the optimization algorithm

In this paper, a two-stage coordinated optimization method of WAPSS parameters based on TLBO algorithm is used to solve the optimal protection scheme for grid wide area. In order to prove that this paper's algorithm has advantages in grid wide area protection, PSO algorithm, TS algorithm, and TS-PSO algorithm are selected as

comparison algorithms to compare the results of protection optimization of grid intervention system in multiple time periods. Based on the observation of the characteristics of the daily load sampling data curves of the three power grids, the time periods of the quadratic segments are divided into [0,6], [6,16], [16,21], [21,24]; the first of the three typical loads, which has the greatest ups and downs and the heaviest loads, is adopted for the division, and the time periods of the octet segments are divided into [1,6], [6,7], [7,10], [10,12], [12. 14], [14, 19], [19, 21], [21, 24]; twenty-four segments are divided into time slots according to the 24 hours of the day. Since the optimization results only once cannot reflect the advantages and disadvantages of which algorithms, under the same initial conditions, the four algorithms are respectively run 35 times randomly according to the 24 segments, and the average of the optimization results of various algorithms is taken for comparison.

Table 3 shows the comparison of the results of different algorithms in 24 time segments. In Table 3, under the initial operating condition, i.e., the distribution system is under grid wide protection, its total system active network loss is 2.406MW, the lowest point voltage of the system is 0.9396, and the node voltage has overrun the limit. After the optimization of this paper's algorithm, the obtained system network loss is 1.841MW, the network loss reduction rate is 23.48%, and there is no over-limit situation of node voltage. The optimization effect of this paper's algorithm is better than several comparison algorithms. At the same time, the calculation time of this paper's algorithm is only 12.1s, which is much smaller than that of the comparison algorithms TS 38.8s, PSO 40.7s and TS-PSO 35.6s. It can be seen that this paper's algorithm not only ensures the optimization effect of the wide-area protection of the grid, but also saves the computation time greatly, which proves the effectiveness of this paper's algorithm.

Table 3: Comparison of different algorithm results in 24 periods

Algorithm	System network loss /MW	System lowest point voltage /pu	System highest point voltage /pu	Calculate time /s
Initial state	2.406	0.9396	1	-
TS	1.977	0.9534	1	38.8
PSO	1.973	0.9531	1	40.7
TS-PSO	1.955	0.9530	1	35.6
TLBO	1.841	0.9292	1	12.1

Note: - indicates that this indicator has no comparative significance in the table

III. B. 2) Simulation of two-stage coordinated optimization of WAPSS parameters based on the algorithm in this paper

Table 4 gives the calculation results of the two-stage coordinated optimization of the parameters of the 4-segment, 8-segment and 24-segment WAPSS. Compared with the initial operating state of the system (without parameter coordinated optimization), there is a corresponding reduction in network loss, and its network loss reduction rate is 17.91%, 18.08% and 23.48%, respectively, and the node minimum voltages of the system operation are all improved compared with the initial operating state of the system. It can be seen that the two-stage coordinated optimization of parameters based on the algorithm of this paper has the effect of reducing the network loss and improving the voltage level for the grid wide system. Moreover, data comparison shows that the finer the daily load data curve is divided, the better the loss reduction effect brought by the two-stage coordinated optimization of WAPSS parameters on it.

Table 4: Calculation results of the method proposed in this paper in different segments

Number of segments	System network loss /MW	System lowest point voltage /pu	System highest point voltage /pu	Network loss reduction rate (Compared with the initial state)
Initial state	2.406	0.9396	1	-
4 sections	1.975	0.9539	1	17.91%
8 sections	1.971	0.9530	1	18.08%
24 segments	1.841	0.9292	1	23.48%

Table 5 shows the comparison of optimization simulation results. The table gives a comparison of the 10 capacitor banks installed for the commissioning cases based on the optimization results of the two-stage coordinated optimization of the WAPSS parameters based on the improved TLBO algorithm for the 4-, 8- and 24-segmented

capacitor banks. In this case, the 8-segmented data 6 (12122111) of C9 in the table indicates a total of 6 changes in the total capacity of the capacitor bank installed at node 9, with the sequence of its capacity changes in parentheses. From the different capacitor casting data in the data in Table 5, it can be concluded that the two-stage coordinated optimization method of WAPSS parameters with time periods divided by sampled load data curves can effectively control the number of actions of grid wide protection devices. In both cases containing the constraints on the number of actions, the coordinated optimization optimization results in more capacitor cuts in a day for 24 segments, and fewer cuts for both 4 and 8 segments. At the same time, the data on the number of capacitor casting times for each compensation point in Table 5 (e.g., the number of actions at compensation point C9 is 7, 7, and 9 for 24 segments) illustrate that the application of the group-optimized casting control strategy for capacitor banks can control the number of times each capacitor in the bank can be cast, preventing the overly-frequent casting of a certain capacitor, and thus enabling the realization of grid wide-area protection.

Table 5: Optimize the comparison of simulation results

Equipment	Number of actions			Equipment	Number of actions		
	4 sections	8 sections	24 sections		4 sections	8 sections	24 sections
C9	3(1224)	6(1212 2111)	14(23211212/1221)	C21	3(1133)	5(1131 3124)	10(12222121/1123 1111/22222111)
C9-1	1	3	7	C21-1	2	3	4
C9-2	1	2	7	C21-2	2	4	4
C9-3	2	3	9	C21-3	1	4	6
C12	3(1230)	4(1121 2213)	14(11122212/3212 2223/32312331)	C24	2(1120)	7(2103 1211)	9(11111112/1122 2212/22212113)
C12-1	1	2	6	C24-1	2	5	4
C12-2	2	3	6	C24-2	1	4	4
C12-3	2	4	7	C24-3	1	3	5
C17	2(1212)	6(1213 1220)	15(11113121/2212 1322/02221312)	C27	2(2111)	4(1120 1121)	10(21111111/1110 2111/12121222)
C17-1	1	2	7	C27-1	2	3	5
C17-2	1	2	7	C27-2	1	2	4
C17-3	2	4	6	C27-3	1	2	4
C19	2(2230)	6(2212 1232)	12(11211211/1221 2221/22223123)	C30	2(1220)	3(1011 2112)	11(11110111/1111 1121/20102211)
C19-1	1	4	5	C30-1	2	3	8
C19-2	1	3	5	C30-2	1	2	6
C19-3	2	4	5				
C15	2(1220)	3(1222 1111)	10(00001201/2212 2211/22111112)	C34	3(0120)	7(1202 0122)	13(12110111/1220 1121/10121112)
C15-1	2	2	7	C34-1	3	5	8
C15-2	1	3	7	C34-2	1	3	9

III. C. Comparison of WAPSS parameters before and after optimization

Since the parameters of the optimization method have a large impact on the optimization effect, in this section, small interference optimization experiments are carried out using motor 1 and motor 2 to compare the level of influence of the parameters on the small interference effect of the motors before and after optimization.

In motor 1, the initial parameters are set as follows: the K-PSS1 and K-PSS2 are 4, the T1-PSS1 and T1-PSS2 are 0.07, and the T2-PSS1 and T2-PSS2 are 0.6. The optimization parameters are set as follows: the K-PSS1 is 4, K-PSS2 is 1.693, the T1-PSS1 is 0.06, T1-PSS2 is 0.0561, T2-PSS1 is 0.7, and T2-PSS2 is 0.658.Fig. 4 shows the comparison of power angle difference of motor 1 before and after parameter optimization. From Fig. 4, it can be seen that the power angle difference of motor 1 after parameter optimization ranges from 42.647 to 58.230, which is smaller than the power angle difference of motor 1 before optimization.

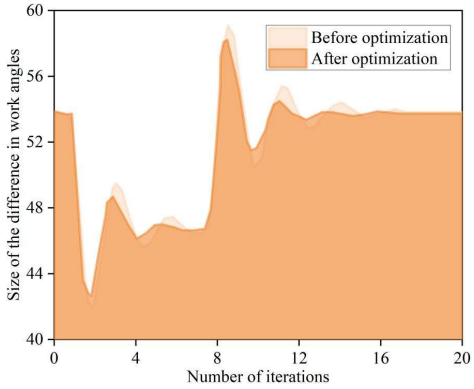

Figure 4: Optimize the power Angle difference of motor 1 before and after

In motor 2, the initial parameters are set as follows: the K-PSS1 and K-PSS2 are 4, the T1-PSS1 and T1-PSS2 are 0.07, and the T2-PSS1 and T2-PSS2 are 0.6. The optimized parameters are set as follows: the K-PSS1 is 2, the K-PSS2 is 4, the T1-PSS1 is 0.08, the T1-PSS2 is 0.0713, the T2- PSS1 is 0.7, T2-PSS2 is 0.580.Fig. 5 shows the comparison of power angle difference of motor 2 before and after parameter optimization. Observing the comparison of power angle difference in Fig. 5, the range of power angle difference of motor 2 after optimization is between 51.374-59.050, which is smaller than the range of power angle difference before optimization. And it is obvious from Fig. 5 that the power angle difference after parameter optimization fluctuates more smoothly in 20 iterations. It indicates that the optimization of the parameters can make the motor obtain a smaller and more stable power angle difference and reduce the amount of losses of the motor in the wide area of the grid.

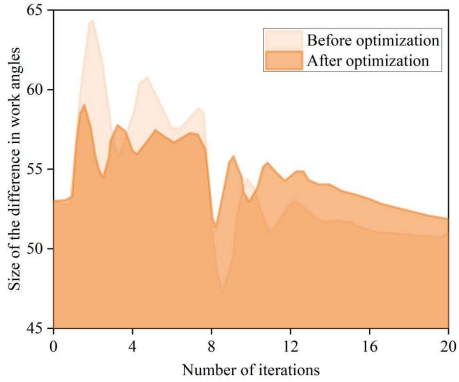

Figure 5: Optimize the power Angle difference of motor 2 before and after

IV. Conclusion

In this paper, we propose the method of fusion data real-time processing and grid protection scheme co-optimization to enhance the effect of grid wide-area protection. In the effect test of sampling data processing algorithm, the errors of steady state recording error and current measurement accuracy are less than 0.55A and 0.55%. The absolute value of three-phase phase difference is $\leqslant$0.55. The error situation meets the requirements. In the simulation experiments of two-phase coordinated optimization of 4-segment, 8-segment and 24-segment WAPSS parameters, the network loss reduction rate of this paper's algorithm reaches 17.91%, 18.08% and 23.48%, respectively, and it can effectively realize the wide-area protection of the power grid. At the same time, the parameter optimization can also make the power angle difference of the grid motor reduce and become more stable. In the future, deep learning and other algorithms can be introduced to realize the dynamic adjustment of parameters, so that the grid intervention protection scheme has real-time, and the intelligent level of grid protection can be enhanced.

Funding

This work was supported by Special Topic 9 of Guangdong's "15th Five Year Plan" New Power System Planning: Research on Guangdong Power Grid's "15th Five Year Plan" Secondary System Planning (Project Number: 031000QQ00240021).

References

[1] Huang, Q., Jing, S., Li, J., Cai, D., Wu, J., & Zhen, W. (2016). Smart substation: State of the art and future development. IEEE Transactions on Power Delivery, 32(2), 1098-1105.

[2] Gaspar, J., Cruz, T., Lam, C. T., & Simões, P. (2023). Smart substation communications and cybersecurity: A comprehensive survey. IEEE communications surveys & tutorials, 25(4), 2456-2493.

[3] Mandal, A., Muttaqi, K. M., Islam, M. R., Sutanto, D., Rahman, A., Yilmaz, O., & Vaze, O. (2025). A Substation Automation System Architecture for Migrating From Decentralized to Centralized Protection and Control in Smart Substations. IEEE Transactions on Industry Applications.

[4] Pavon, W., Inga, E., Simani, S., & Nonato, M. (2021). A review on optimal control for the smart grid electrical substation enhancing transition stability. Energies, 14(24), 8451.

[5] Ni, C., Li, R., Deng, M., Li, X., Li, W., Su, Y., & Li, B. (2019, October). Research on the Application of Smart Substation Area Protection. In 2019 IEEE 8th International Conference on Advanced Power System Automation and Protection (APAP) (pp. 125-129). IEEE.

[6] Hossain, M. S., Rahman, M., Sarker, M. T., Haque, M. E., & Jahid, A. (2019). A smart IoT based system for monitoring and controlling the sub-station equipment. Internet of things, 7, 100085.

[7] Nan, D., Wang, W., Mahfoud, R. J., Haes Alhelou, H., Siano, P., Parente, M., & Zhang, L. (2020). Risk assessment of smart substation relay protection system based on markov model and risk transfer network. Energies, 13(7), 1777.

[8] Zhao, B., Yang, C., Wang, Y., & Wang, H. (2017, December). Functions and implementation of substation-area backup protection in smart substation. In 2017 IEEE 2nd Information Technology, Networking, Electronic and Automation Control Conference (ITNEC) (pp. 218-222). IEEE.

[9] Zhang, X., Ma, H., & Chi, K. T. (2022). Assessing the robustness of cyber-physical power systems by considering wide-area protection functions. IEEE Journal on Emerging and Selected Topics in Circuits and Systems, 12(1), 107-114.

[10] Eissa, M. M. (2018). A new wide-area protection scheme for single-and double-circuit lines using 3-D-phase surface. IEEE Transactions on Power Delivery, 33(6), 2613-2623.

[11] Vahidi, S., Ghafouri, M., Au, M., Kassouf, M., Mohammadi, A., & Debbabi, M. (2023). Security of wide-area monitoring, protection, and control (WAMPAC) systems of the smart grid: A survey on challenges and opportunities. IEEE Communications Surveys & Tutorials, 25(2), 1294-1335.

[12] Babu, N. P., Babu, P. S., & SivaSarma, D. V. S. S. (2015, June). A wide-area prospective on power system protection: A state-of-art. In 2015 international conference on energy, power and environment: towards sustainable growth (ICEPE) (pp. 1-6). IEEE.

[13] Ashok, A., Govindarasu, M., & Wang, J. (2017). Cyber-physical attack-resilient wide-area monitoring, protection, and control for the power grid. Proceedings of the IEEE, 105(7), 1389-1407.

[14] Wang, Q., Bo, Z., Zhao, Y., Ma, X., Zhang, M., Zheng, H., & Wang, L. (2019). Integrated wide area protection and control for power grid security. CSEE Journal of Power and Energy Systems, 5(2), 206-214.

[15] Bindra, A. (2017). Securing the power grid: Protecting smart grids and connected power systems from cyberattacks. IEEE Power Electronics Magazine, 4(3), 20-27.

[16] Ashok, V., Yadav, A., & Abdelaziz, A. Y. (2020). A comprehensive review on wide-area protection, control and monitoring systems. Wide Area power systems stability, protection, and security, 1-43.

[17] Wu, S. (2017). An adaptive limited wide area differential protection for power grid with micro-sources. Protection and Control of Modern Power Systems, 2(3), 1-9.

[18] Kundu, P., & Pradhan, A. K. (2017). Power network protection using wide-area measurements considering uncertainty in data availability. IEEE Systems Journal, 12(4), 3358-3368.